Scientific Paper / Artículo Científico

UNIVERSIDAD POLITÉCNICA SALESIANA ECUADOR
INGENIUS
Revista de Ciencia y Tecnología
https://doi.org/10.17163/ings.n34.2025.10
pISSN: 1390-650X / eISSN: 1390-860X

Implementation and evaluation of a wheeled-legged locomotion robot for optimizing the preflight air intake inspection protocol of fighter aircraft

Implementación y evaluación de un robot con sistema de locomoción *wheeled-legged* para la optimización del protocolo de inspección de tomas de aire en aviones caza en estado previo al vuelo

Mayki Mamani[1,*], Jhonathan Uchamaco[1], David Meneses[1], Yuri Silva[1], Jorge Apaza[1]

Received: 12-05-2025, Received after review: 02-06-2025, Accepted: 11-06-2025, Published: 01-07-2025

Abstract

Maintenance and inspection protocols in the aerospace industry are designed to safeguard the structural integrity of aircraft and ensure pilot safety. However, the air intakes of fighter aircraft pose significant access challenges for maintenance technicians during preflight inspections. To address this limitation, this study presents an innovative solution: the implementation and evaluation of a robot equipped with a wheeled-legged locomotion system. This system enables efficient access to the air intakes, significantly enhancing the inspection protocol. The robot was developed in close alignment with the operational requirements of Peruvian Air Force (FAP) technicians, which was critical to defining its design specifications and manufacturing parameters. Its adaptive and compact architecture allows it to navigate confined intake structures effectively, optimizing inspection time and resource utilization. The prototype's performance was rigorously assessed through standardized tests, demonstrating its capability to reliably access and inspect air intakes under preflight conditions. This advancement contributes to the modernization of conventional aircraft maintenance procedures by integrating robotic technologies into the aeronautical inspection process.

Keywords: Robot, design, inspection, air intake, fighter aircraft, locomotion, wheeled-legged

Resumen

Los protocolos de mantenimiento e inspección en la industria aeroespacial están diseñados para salvaguardar la integridad estructural de las aeronaves y la seguridad de los pilotos. Las tomas de aire de los aviones caza presentan un acceso limitado para los técnicos de mantenimiento durante la inspección en estado previo al vuelo. Ante esta limitación, se propone una solución innovadora mediante la implementación de un robot con sistema de locomoción *wheeled-legged*, que permite acceder a dichas tomas de aire y optimizar significativamente el protocolo de inspección. En esta investigación se desarrolló e implementó un robot con tecnología de locomoción *wheeled-legged*, cuyo propósito específico es facilitar la inspección de las tomas de aire en aviones caza previo al vuelo. Para su diseño y fabricación se consideraron cuidadosamente los requerimientos operativos de los técnicos de la Fuerza Aérea del Perú (FAP), lo que resultó fundamental en la definición de las especificaciones del sistema. El resultado fue un diseño adaptativo y compacto que permite al robot desplazarse con eficacia a través de las tomas de aire, optimizando el tiempo y los recursos empleados en las inspecciones. Mediante pruebas estandarizadas se evaluó el rendimiento del prototipo, demostrando su capacidad para acceder e inspeccionar eficazmente dichas estructuras. Esto permite mejorar el protocolo de mantenimiento tradicional mediante la incorporación de tecnología avanzada en los procesos de inspección aeronáutica.

Palabras clave: robot, diseño, inspección, tomas de aire, aviones caza, locomoción, wheeled-legged

[1,*]Mechanical Engineering Professional School, Production and Services Faculty, Universidad Nacional de San Agustín de Arequipa, Arequipa, Perú. Corresponding author ✉: mmamanimar@unsa.edu.pe.

Suggested citation: M. Mamani, J. Uchamaco, D. Meneses, Y. Silva and J. Apaza, "Implementation and evaluation of a wheeled-legged locomotion robot for optimizing the preflight air intake inspection protocol of fighter aircraft," *Ingenius, Revista de Ciencia y Tecnología*, N.° 34, pp. 126-139, 2025, DOI: https://doi.org/10.17163/ings.n34.2025.10.

1. Introduction

Currently, in the aeronautical industry, the optimal performance of aircraft is ensured through specialized maintenance protocols designed to uphold the highest safety standards [1]. Among the critical components addressed in these procedures are the air intakes. These structures, characterized by their complex geometry, contain multiple peripheral gates that redirect airflow toward the engine, thereby enhancing the aircraft's overall performance [2] and [3].

In the Peruvian Air Force (FAP), accessing the air intakes of fighter aircraft presents specific challenges that complicate inspection tasks for maintenance personnel. This limitation can result in overlooked structural defects or the presence of foreign object debris (FOD) [4], posing a significant risk of catastrophic incidents, potential loss of life, and substantial material damage with severe economic repercussions [5].

In the FAP, daily and weekly maintenance routines include engine removal to facilitate thorough inspection of the air intakes [6]. However, during preflight inspections, the available time is limited, and disassembling the engine is impractical, which prevents technicians from adequately inspecting the air intakes [7].

The use of periscopes as tools to visually access hard-to-inspect areas of aircraft has been explored and implemented within the FAP. However, their limited reach and the complex geometry of the air intakes continue to pose a risk of undetected fuselage defects or the presence of FOD [8,9]. Although these devices provide partial enhancements to maintenance protocols, the possibility of missed faults during the preflight phase remains.

On the other hand, advances in additive manufacturing technologies, such as 3D printing, have grown significantly across various industrial sectors [10], particularly in robotics, where they enable the rapid and cost-effective creation of complex designs for inspecting hard-to-reach areas [11–15].

Similarly, robotics has been increasingly integrated into aircraft maintenance processes. Notable examples include the use of unmanned aerial vehicles (UAVs) for aircraft inspections by the Spanish Air Force in collaboration with Airbus [16]; the application of vortex technology for inspecting fuselages and wings [17]; octopod robots capable of adhering to aircraft surfaces to inspect rivets [18,19]; the development of continuum robots that navigate cavities to inspect engines [20,21]; and modular robots designed to examine the interior of wings and their internal structures [22].

Although these technologies have been explored for general aircraft maintenance, they do not specifically address the inspection of air intakes, which are confined spaces with complex geometries and limited accessibility. Currently, there is a lack of studies and experimental validation supporting the deployment of robots within these structures.

To address this limitation, various locomotion technologies have been investigated for accessing air intakes, including tracks, conventional wheels, adaptive designs, omnidirectional systems, continuum robots, electroadhesive mechanisms, and unmanned aerial vehicles (UAVs) [23]. Among these alternatives, wheeled-legged locomotion technology stands out [24], as it combines wheels and legs in mobile platforms, enabling stable movement over irregular surfaces such as those found inside air intakes.

This approach is supported by developments such as the Centauro robot from the German Aerospace Center (DLR), which employs a hybrid locomotion system to operate on rough terrain during search and rescue missions [25]; and the Roller Walker [26], which combines wheels for movement on smooth surfaces with articulated legs to overcome obstacles. However, none of these systems have been designed for the deployment of hybrid robots within confined spaces inside aircraft.

This study presents the implementation and evaluation of the ALLQU robot, equipped with a wheeled-legged locomotion system designed to optimize maintenance protocols by enabling access to and inspection of air intakes. For its validation, three methodological frameworks are employed: the NIST-ASTM testing protocol for evaluating robots in complex environments [23]; the FAP POCHE maintenance protocol; and the NASA TLX methodology, which analyzes operator workload to assess the system's usability, advantages, and limitations within the operational context.

2. Materials and methods

2.1. Wheeled-Legged Robots

As illustrated in Figure 1, wheeled-legged robots combine wheels and legs to enhance mobility across varied terrains. These systems employ actuators that enable switching between different locomotion modes depending on the terrain characteristics. However, this versatility can increase operational complexity, an aspect evaluated in this study using the NASA TLX methodology [27].

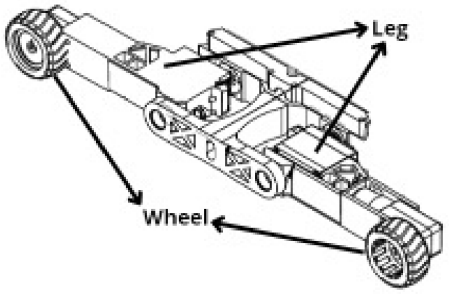

Figure 1. Wheeled-legged robot

Some of the advantages and disadvantages of this type of robot, as reported by Li et al. [27], are summarized in Table 1.

In general, their adaptability and stability, defined as the ability to maintain position and orientation without tipping over or excessive slipping, make them a suitable option for applications in hard-to-reach environments, such as the one addressed in this study.

Table 1. Examples of wheeled-legged robots

Previous work		Characteristics
[28]	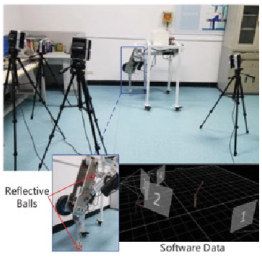	
[29]	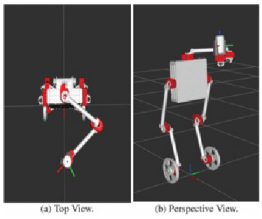	
[30]	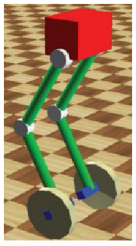	**Advantages** High mobility High stability Great obstacle avoidance capability **Disadvantages** High level of control required
[31]	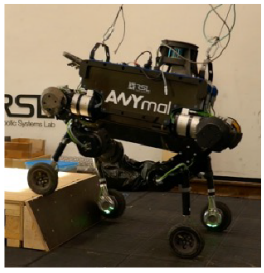	
[32]	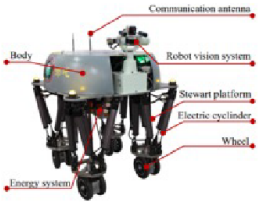	

2.2. Study of the Work Environment

The air intake environment of the Mirage 2000, whose structure is primarily composed of aluminum, was analyzed. Its location is shown in Figure 2(a), and its main components, including inlets, outlets, gates, and critical sections, are mapped in Figure 2(b).

The air intake entrance has a height of 16 cm Figure 2(c), while the outlet, which connects to the compressor area, has a diameter of 78 cm Figure 2(d). In one critical section, the maximum recorded height is 14 cm.

Peripheral Gate 1 features a drop of 12 cm, an opening of 35 cm, and a slope of 30° Figure 2(e), whereas Gate2 has a height of 5 cm Figure 2(f).

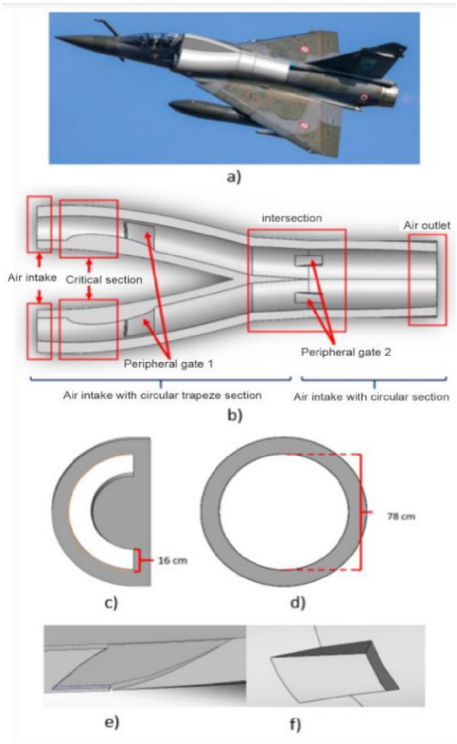

Figure 2. Characteristics of the air intakes of Mirage 2000 fighter aircraft: (a) Location of the air intake on the fighter aircraft [**?**]. (b) Components of the air intake. (c) Section at the air intake entrance. (d) Section at the air intake outlet. (e) Peripheral Gate 1. (f) Peripheral Gate 2.

The preflight maintenance protocol for the Mirage 2000, as outlined in the POCHE manual, includes six main components, which are shown in Figure 3. Among these, the air intake, characterized by restricted access, constitutes the primary focus of this study.

Maintenance includes inspecting the internal fuselage, verifying that the gates are properly closed, and ensuring the absence of FOD within the system.

The requirements of FAP technical personnel were collected and analyzed through surveys and structured interviews, using rating scales. The results were classified into two categories: technical requirements (dimensions, reach, FOD detection, stability, maneuverability, and speed) and economic requirements (cost and availability).

Interviews were conducted with three key groups of FAP personnel involved in the inspection of air intakes:

1. Technicians responsible for the manual inspection of the aircraft.

2. Personnel responsible for the removal of foreign objects.

3. Supervisors responsible for documenting and recording inspection activities.

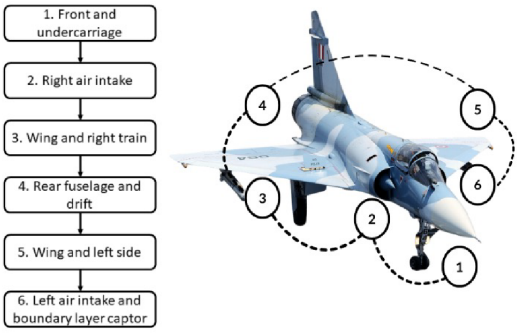

Figure 3. Preflight maintenance procedure for Mirage 2000 fighter aircraft.

The averages obtained from the surveys and interviews are presented in Table 2. The final score represents the mean value of both sources and is illustrated in the bar chart in Figure 4.

The order of importance assigned to the evaluated criteria for the prototype design was as follows: Effectiveness (4.8), Reach (4.6), Maneuverability (4.4), Adaptability (4.05), Dimensions (3.5), Availability (3.4), Stability (2), Speed (1.15), and Cost (0).

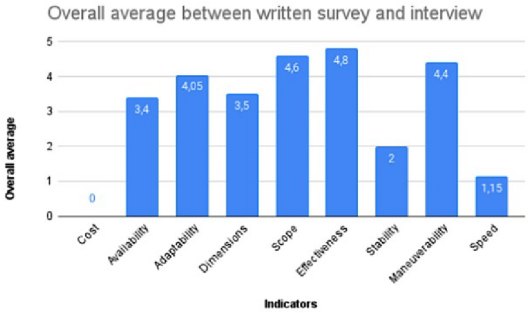

Figure 4. Average scores from the written surveys and interviews of FAP personnel

Table 2. Analysis of results from the written surveys and interviews

Indicator	Average		Overall Average
	Written sruvey	Interview	
Cost	0	0	0
Availability	3.3	3.5	3.4
Adaptability	3.8	4.3	4.05
Dimensions	3	4	3.5
Range	4.6	4.6	4.6
Effectiveness	4.8	4.8	4.8
Stability	4	0	2
Maneuverability	4.1	4.7	4.4
Speed	2.3	0	1.15

Note: The score ranges from 1 to 5 depending on of growing importance.

Based on the analysis of the air intake environment, the FAP's preflight maintenance protocol, and the results of surveys and interviews with technical personnel, the requirements that the ALLQU robot must meet were defined and are presented in Table 3.

Table 3. List of requirements

Characteristic	Requirement
Main function	Inspection of the internal fuselage of the air intakes and detection of FOD
Dimensioning	The size of the robot is based on the critical section, with a height of up to 140 mm and a minimum length of 350 mm.
Mobility	Movement throughout the interior of the air intakes.
Adaptability	The system must adapt to the shape of the air intake.
Stability	The robot must be stable throughout its entire journey.

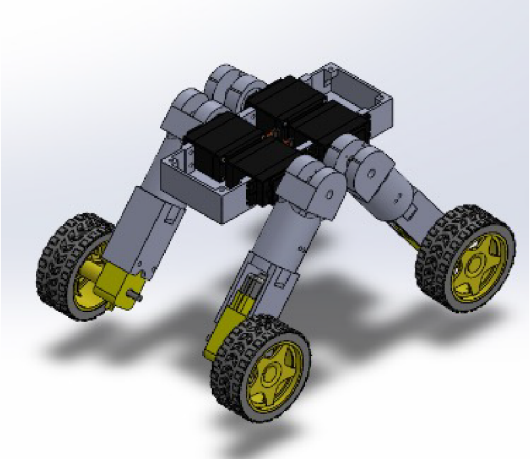

Figure 6. Three-dimensional assembly of the ALLQU robot in SolidWorks.

3. Results and discussion

3.1. Design, Construction, and Implementation of a Robot with a Wheeled-Legged System

Based on the established requirements, the robot's dimensions are shown in Figure 5: a maximum height of 140 mm, a width of 250 mm, and a length of 400 mm. The length slightly exceeds the 350 mm opening of Peripheral Gate 1, ensuring that the robot can pass through this section without the risk of jamming.

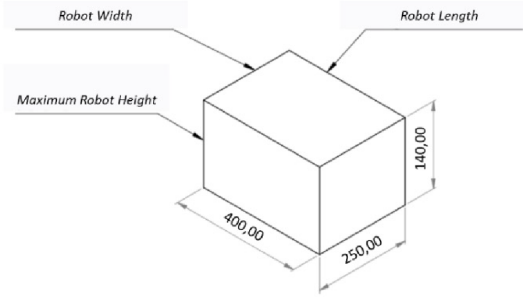

Figure 5. Conceptual dimensions of the robot relative to the available space in the critical section of the Mirage 2000 fighter aircraft air intake

3.2. Design of the wheeled-legged system

The design and assembly of the ALLQU robot's mechanical components were performed using three-dimensional modeling software, as illustrated in Figure 6. The design prioritizes compactness and adaptability, which are essential for operationin confined spaces.

A hybrid wheeled-legged locomotion system was selected for its demonstrated ability to combine the efficiency of wheels with the adaptability of legs. This configuration enables the robot to contract and extend its structure, ensuring stable and efficient movement through the complex geometries of the air intakes, including peripheral gates and critical sections.

To balance weight, strength, and functionality, 14 lightweight yet robust structural components were fabricated using 3D printing. The final design has a total weight of 1.350 kg and dimensions of 140 mm in height, 250 mm in width, and 400 mm in length, ensuring precise adaptation to the critical section, which has a height of 14 cm and a 35 cm opening at Peripheral Gate1.

This configuration was designed to maximize maneuverability and access capability in restricted environments while balancing these attributes against the inherent complexity of control and manufacturing cost.

The robot comprises six main mechanical components, as illustrated in Figure 7. It is equipped with four rubber wheels, each with a radius of 22.5 mm, which are mounted using the couplings shown in Figure 7(a) that connect them to the geared motors.

The structural legs, which support the motors, are shown in Figure 7(b) and are attached to pivots, as depicted in Figure 7(c), allowing movement via independent servomotors. The chassis, shown in Figure 7(d), provides structural stability and overall support for the assembly. The cover, shown in Figure 7(e), protects the servomotors and serves as a mount for the electronic system, which is housed within the module shown in Figure 7(f).

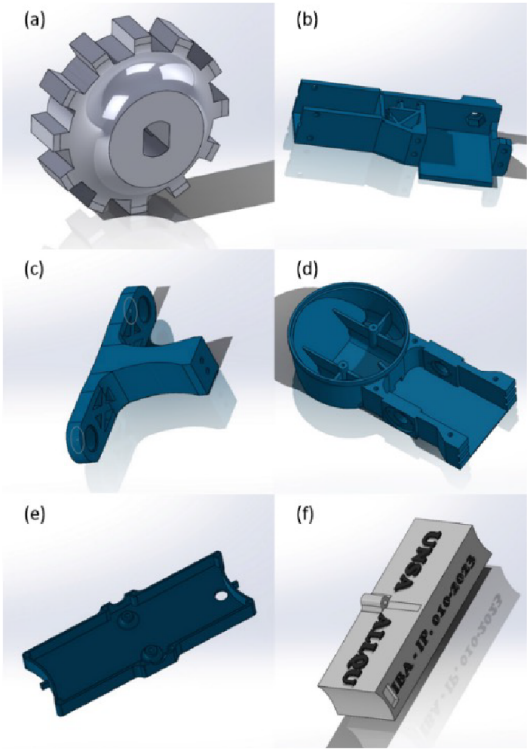

Figure 7. Three-dimensional modeling of the ALLQU robot components in SolidWorks: (a) Wheel coupling, (b) Leg, (c) Pivot structure, (d) Chassis, (e) Cover, (f) Electronics module

Two operational scenarios were evaluated in the critical section of the system, as shown in Figure 8: the robot's entry with all four wheels on a 30° slope Figure 8(a), and its exit with two wheels on a flat surface Figure 8(b).

With a mass of 1.35 kg and static and rolling friction coefficients of $C_f = 0.74$ and $C_r = 0.005$, respectively, the required forces were calculated to be 6.679 N for ascending the incline and 0.066 N for movement on a flat surface. Considering a wheel radius of 22.5 mm, the required torque was determined to be 0.038 Nm, which is below the maximum allowable limit of 0.052 Nm, thereby ensuring sufficient traction and preventing slippage.

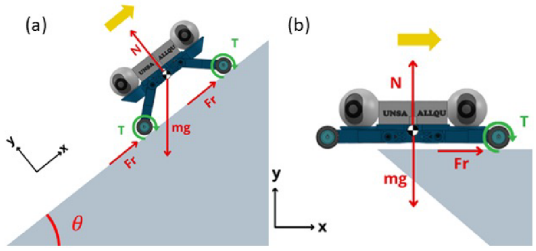

Figure 8. Free body diagram of the robot: (a) Inclined at 30° with 4 wheels in contact, (b) Horizontal plane at 0° with 2 wheels in contact

Table 4. Required torque values

Torques	Description	Torque Parameters (Nm)
Torque on motor of wheels required	2 wheels in contact and inclination 0º.	Treq 0º = 0,002 Nm
	4 wheels in contact or inclination 30º.	Treq 45º = 0,038 Nm
Maximum torque of wheel tractions	2 wheels in contact nd inclination 0º.	Tmax.tractivo 0º = 0,104 Nm
	4 wheels in contact and inclination 30º.	Tmax.tractivo 45º = 0,052 Nm

The robot's movement was simulated in the critical section of the air intake (Figure 9). The simulation confirmed that its dimensions, along with the wheeled-legged system, allow it to traverse this section effectively.

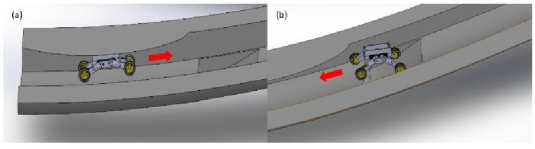

Figure 9. SolidWorks motion simulation of the robot in the critical section of the air intake: (a) Robot entry, (b) Robot exit.

Figure 9(a) shows the robot's entry using only its wheels, while Figure 9(b) depicts its exit using its legs.

3.3. Construction and implementation

The ALLQU robot was constructed in the manufacturing laboratory of the National University of San Agustín de Arequipa, as shown in Figure 10. The design includes a total of 14 structural components fabricated using 3D printing, along with 4 wheel couplings, 4 legs, 2 pivots, 2 chassis structures, a cover, and a central electronic module.

The robot is equipped with 4 high-grip rubber wheels, coupled to 3–6 V DC gear motors. Each leg

is driven by 4.8–7.2 V DC servomotors. Additionally, it has 2 wireless cameras with integrated LED and infrared lighting systems to facilitate inspections in low-visibility environments.

Figure 10. Assembly of the ALLQU robot

The dimensions of the ALLQU robot and the Operational Control Unit (OCU) are shown in Figure 11 and detailed in Table 5. These measurements were recorded with the robot in its extended configuration, as depicted in Figure 8(b). The resulting dimensions enable effective maneuvering in confined spaces, such as the air intakes of fighter aircraft.

Figure 11. ALLQU robot and Operational Control Unit (OCU)

Table 5. Specifications of the ALLQU robot and THE Operational Control Unit (OCU)

Characteristics	Description	Parameter
Robot characteristics	Robot weight	1,350 kg
	Robot length	350 mm
	Robot width	150 mm
	Robot height	110 mm
Operator Control Unit (OCU) characteristics	Weight OCU	300 grams
	length OCU	150 mm
	width OCU	175 mm
	height OCU	40 mm

The robot's structure, built from 3D-printed components, is lightweight and durable, which enhances operational efficiency. The integrated cameras, described in Table 6, were specifically selected to enable recording in low-light conditions, such as those inside the Mirage 2000 air intake.

Table 6. Camera Characteristics

Description	Parameter
Connectivity technology	Wireless
Connectivity protocol	Wifi
Camera weight	20 grams
Light source type	LED e infrared
Power	15 watts

The assembled version of the ALLQU robot is shown in Figure 12, which also illustrates the maximum angles that can be formed between the legs and the body of the system. In Figure 12(a), an angle of 70° is observed when the legs are positioned below the body. In Figure 12(b), angles of 25° between the body and the front leg in the upward direction, and 15° between the body and the rear leg in the same direction, are measured.

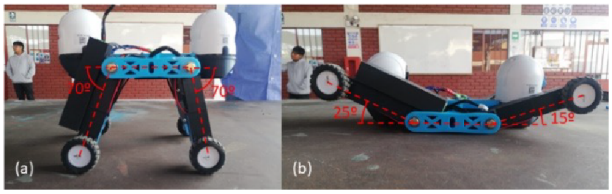

Figure 12. ALLQU robot with wheeled-legged locomotion system: (a) Maximum angle between the body and the legs in the downward position. (b) Maximum angles between the body and the legs in the upward position

Table 7 presents the technical specifications of the robot.

Table 7. Especificaciones técnicas del robot

Characteristics	Description
Type of locomotion	Wheeled-Legged
Robot dimensions	Length: 350 mm
	Width: 150 mm
	Height: 110 mm
Robot weight	1,350 kg
Wheels	4 rubber wheels
	Radius: 22,5 mm
Legs	4 servomotors
Inspection cameras	2 wireless cameras
Connectivity	Wifi
Camera weight	20 g
Light source (camera)	Infrared LED
Power (camera)	15W
OCU dimensions	Length: 150 mm
	Width: 175 mm
	Height: 40 mm
OCU weight	300 g

3.4. Analysis of the Test Setup and Testing Methodology

This section describes the characteristics of the two tests conducted on the ALLQU robot. The first test evaluates the turning performance of the wheeled-legged system and the camera's effectiveness under real operating conditions. The second test assesses the overall performance of the wheeled-legged locomotion system and the mental workload perceived by the operator while controlling the robot.

3.4.1. Test of the turning effectiveness of the wheeled-legged system and camera performance

A ventilation duct was used, as shown in Figure 13 and detailed in Table 8, to simulate a narrow space with low lighting conditions. This environment enabled the evaluation of the ALLQU robot's turning capability and the quality of the video captured by its camera.

Figure 13. Ventilation duct used for the tests

The test was repeated ten times, varying the angles between the robot's body and its legs. Subsequently, the robot advanced toward the chart, capturing images at different distances, and then returned to the starting point along the same path.

Table 8. Characteristics of the ventilation duct

Characteristics	Value
Profile	Circular
Length	1,83 m
Diameter	0,62 m
Surface material	Steel

3.4.2. Test of the effectiveness of the wheeled-legged locomotion system and analysis of mental workload using NASA TLX

The test of the wheeled-legged locomotion system and the operator's mental workload was conducted at the air base, specifically at the air intakes of the Mirage 2000. Due to the environmental conditions, there were limitations on both the test range and the number of trials performed. Details of the experimental environment are illustrated in Figure 14.

The evaluation included an analysis of displacement effectiveness and travel time in the sections previously identified in Figure 2: the two lateral air intakes and the central intersection. Following the FAP's POCHE maintenance protocol, the robot was initially positioned at the right intake, moved toward the intersection, and then returned through the left intake.

Eight tests were conducted with four trained operators. Subsequently, the NASA TLX methodology was applied to assess the mental workload perceived by the participants, taking into account factors such as physical and mental effort, perceived performance, frustration level, and the demands of the operational environment.

Figure 14. Ventilation duct of the Mirage aircraft

3.5. Results Analysis

This section presents the results obtained from the tests conducted with the robot equipped with the wheeled-legged locomotion system, as described previously.

3.5.1. Test of the turning effectiveness of the wheeled-legged system and camera performance

The turning effectiveness of the ALLQU robot and the performance of the integrated camera were evaluated. For the turning test, ten trials were conducted inside the ventilation duct, using different angles between the robot's body and its legs oriented toward its underside.

The results are presented in Table 9, detailing the robot's turning performance under the described conditions.

Table 9 shows that the ALLQU robot can perform turns effectively when the angle between the body and the legs exceeds 50°. However, it fails to complete a turn at angles below 45° due to the physical constraints of the test environment. The turning capability is directly influenced by the available space and becomes increasingly limited in narrower areas.

Table 9. Results of the robot turning test

Angle between legs and body	Turn achieved?
70°	Yes
65°	Yes
60°	Yes
55°	Yes
50°	Yes
45°	No
40°	No
35°	No
30°	No
25°	No

Figure 15 shows the test conducted using the Snellen chart and an example of an image captured by the robot's camera. The visual acuity results from this evaluation are summarized in Table 10.

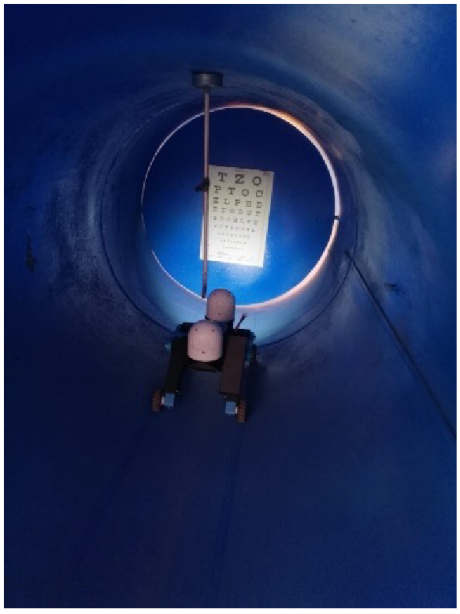

Figure 15. ALLQU robot in the ventilation duct, performing vision tests using a SNELLEN chart.

The visual acuity achieved by the robot's camera varied depending on the light source, distance, and use of zoom. With LED lighting and at a distance of 0.4 m, an acuity of 20/12.5 was achieved, both with and without zoom. At 1.5m , the acuity was 20/20 without zoom, improving to 20/16 when zoom was activated, demonstrating its effectiveness at greater distances.

Under infrared lighting at 0.4 m, the visual acuity was likewise 20/12.5 in both cases. At 1.5 m without zoom, a value of 20/16 was recorded, which remained unchanged when zoom was applied.

These results indicate that the robot's vision system performs reliably at short distances, while the use of zoom significantly enhances visual accuracy at longer ranges. Overall, the system demonstrates robust adaptability to varying lighting conditions and environments.

Table 10. Resultados de prueba de giro del robot

Light source type	Distance	Zoom	Visual acuity	Last letter
LED	0,4 m	No	20/12,5	P
		Yes	20/12,5	P
	1,5 m	No	20/20	P
		Yes	20/16	E
Infrared	0,4 m	No	20/12,5	P
		Yes	20/12,5	P
	1,5 m	No	20/16	E
		Yes	20/16	E

3.5.2. Test of the effectiveness of the wheeled-legged locomotion system and analysis of mental workload using NASA TLX

A test consisting of eight runs performed by four operators was conducted to evaluate the effectiveness of the wheeled-legged locomotion system within the air intakes of the Mirage 2000, following the POCHE protocol established by the FAP. Figure 16 illustrates the robot's positions during the runs.

The results of this locomotion test, including system effectiveness, distances traveled, and travel times, are presented in Table 11.

The operation of the robot by four operators in the air intakes of the Mirage 2000, as shown in Figure 17, was assessed using the NASA TLX methodology. The results include the individual scores, the pairwise comparison chart used to calculate the weighted score, and the final ranking of mental workload.

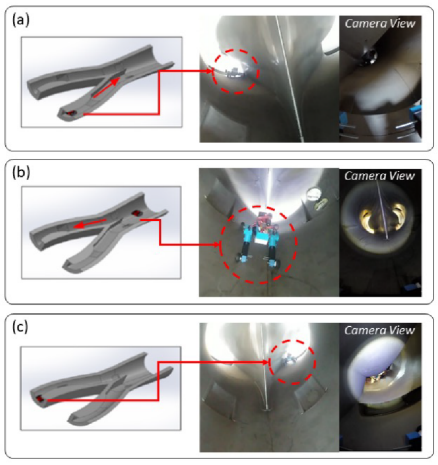

Figure 16. ALLQU robot in the air intake of a Mirage 2000 fighter aircraft, conducting locomotion and inspection tests: (a) Robot entering through the right air intake. (b) Robot at the intersection. (c) Robot exiting through the left air intake

Table 11. Locomotion test results in the air intake of a fighter aircraft

Air intake component	Distance Traveled	Time	Remarks
Right air intake	0,94 m	55,6 s	The circuit was
Engine intersection	3,36 m	36,4 s	completed in
Left air intake	0,94 m	48,7 s	all 8 trials.

Figure 17. Operators preparing the tests

These results are presented in Tables 12, 13, and 14, respectively.

Table 12. NASA TLX methodology scores

Dimension	Person 1	Person 2	Person 3	Person 4
Mental demand	12	20	10	20
Physical demand	4	20	5	17
Temporal demand	12	20	13	14
Performance	20	20	16	18
Effort	14	20	11	18
Frustration level	10	10	15	10

Table 12 shows that the perceived mental and physical workload varied among participants, with Person 2 reporting the highest values in most of the evaluated categories. Temporal demands showed moderate variation, while performance was consistently high, particularly for Persons 1 and 2, who achieved the maximum score of 20.

Effort and frustration levels also varied among operators; however, frustration remained generally low. Overall, these results indicate a high workload accompanied by a moderate emotional response from the participants.

Table 13 presents the weighting values assigned to each dimension of the NASA TLX index, reflecting the perceived importance of each factor contributing to workload. Temporal demand received the highest relative weight, particularly for Person 1 (weight 5) and Person 3 (weight 4), due to the times exceeding 30 seconds recorded in the critical sections of the route.

Mental demand also stood out, with Person 4 assigning it a weight of 4. Frustration had a greater impact on Persons 3 and 4, while physical demand was more significant for Persons 1 and 2.

Table 13. Pairwise comparison chart

Dimension	Person 1	Person 2	Person 3	Person 4
Mental demand	3	2	2	4
Physical demand	1	4	0	0
Temporal demand	5	4	4	1
Performance	4	1	2	3
Effort	2	1	3	4
Frustration level	0	3	4	3

Table 14 shows a high mental workload for most participants, except for Person 3, who recorded a medium level of 985 units. This difference is attributed to the robot's operation in the critical section, as illustrated in Figure 2(b). The tests conducted in both the ventilation duct and the Mirage 2000 validated the operational performance of the ALLQU robot and confirmed the user's perception of cognitive workload.

Table 14. Carga de trabajo mental

Mental workload level	Person 1	Person 2	Person 3	Person 4
Low				
Medium			985	
High	1040	1350		1250

The robot demonstrated its capability to optimize inspection time, reducing both aircraft downtime and the need for highly specialized personnel. The standardized tests were conducted in two scenarios:

1. Turning and vision test, performed in a circular steel ventilation duct with a diameter of 0.62 m and a length of 1.83 m under low-light conditions. A Snellen chart was used to assess the image quality captured by the robot's camera.

2. Locomotion and mental workload test, carried out in the air intakes of an operational Mirage 2000 fighter aircraft located in a FAP hangar. This test evaluated the robot's performance in critical inlet geometries, such as sections with a height of 16 cm and an outlet width of 78 cm, under real field conditions defined by the POCHE protocol.

4. Conclusions

This work presented the development and implementation of the ALLQU robot, equipped with a wheeled-legged locomotion system, specifically designed to enhance preflight inspection of air intakes in fighter aircraft. The robot demonstrated its effectiveness in navigating and inspecting these confined structures, optimizing maintenance resources by reducing aircraft downtime and the need for highly specialized personnel, as validated through tests conducted in a controlled ventilation duct and within the air intakes of an operational Mirage 2000 fighter aircraft.

The main findings of this study are summarized as follows:

- The wheeled-legged locomotion system enabled stable and reliable movement within all three evaluated sections of the Mirage 2000, with average traversal times of 36.4 at the engine intersection and 52.15 s in the lateral air intakes.

- Turning capability in confined spaces was directly dependent on the available area. In a duct with a diameter of 0.62 m, turning was feasible only when the body-to-leg angle exceeded 50°.

- The visual system, comprising optical sensors with integrated LED and infrared lighting, delivered high visual acuity even under low-light conditions. The optical zoom significantly enhanced resolution in areas with limited visibility.

The NASA TLX analysis indicated a high mental workload, particularly in critical sections of the route where operators were required to control multiple elements of the robot simultaneously.

The experimental results confirm the operational feasibility of the ALLQU robot for air intake inspection in fighter aircraft; however, certain technical limitations were identified, including:

- Limited turning ability at angles below45°.

- Visual inspection limited to surface-level observation, with no subsurface detection.

- Limited operational autonomy due to current battery capacity.

- Structural robustness not yet validated under extreme environments (high temperatures, dust, or vibrations).

- High cognitive load on the operator when maneuvering in critical sections.

To address these limitations, future improvements should focus on developing more agile control algorithms, integrating non-destructive testing (NDT) sensors, extending energy autonomy, validating structural performance under diverse operational conditions, and designing a more intuitive user interface to reduce the operator's mental workload.

Beyond its operational efficiency, the ALLQU robot offers qualitative advantages over traditional methods. It reduces the risks associated with manual inspection in confined spaces and provides consistent, objective visual records that improve traceability and support long-term monitoring of potential structural anomalies.

Conflict of Interest

The authors declare that they have no conflict of interest regarding the development of this research. All tests were conducted directly on the developed robot and did not involve human subjects.

Funding

This work is part of the research project "Prototype of an inspection robot for fighter aircraft air intakes during preflight," funded by the Universidad Nacional de San Agustín de Arequipa under contract number PI-010-2023-UNSA.

Acknowledgments

The authors express their deepest gratitude to the Universidad Nacional de San Agustín de Arequipa for its invaluable support throughout this research. Its commitment and backing were essential to the project's development and success.

The authors also thank the Communications and Electronics Squadron and the Aircraft Maintenance Squadron of Air Group No. 4 of the Peruvian Air Force, whose support was crucial for conducting the necessary tests and advancing this research.

Contributor Roles

- **Mayki Mamani**: Methodology, writing – original draft.
- **Jhonathan Uchamaco**: Methodology, writing – original draft.
- **David Meneses**: Validation, visualization.
- **Yuri Silva**: Writing – review & editing, visualization.
- **Jorge Apaza**: Validation, visualization.

References

[1] V. Madonna, P. Giangrande, and M. Galea, "Electrical power generation in aircraft: Review, challenges, and opportunities," *IEEE Transactions on Transportation Electrification*, vol. 4, no. 3, pp. 646–659, Sep. 2018. [Online]. Available: http://doi.org/10.1109/TTE.2018.2834142

[2] A. V. Chatzi, "Safety management systems: an opportunity and a challenge for military aviation organisations," *Aircraft Engineering and Aerospace Technology*, vol. 91, no. 1, pp. 190–196, Jan. 2018. [Online]. Available: http://doi.org/10.1108/AEAT-05-2018-0146

[3] Y. D. Yasuda, F. A. Cappabianco, L. E. G. Martins, and J. A. Gripp, "Aircraft visual inspection: A systematic literature review," *Computers in Industry*, vol. 141, p. 103695, Oct. 2022. [Online]. Available: https://doi.org/10.1016/j.compind.2022.103695

[4] T. Chauhan, C. Goyal, D. Kumari, and A. K. Thakur, "A review on foreign object debris/damage (FOD) and its effects on aviation industry," *Materials Today: Proceedings*, vol. 33, pp. 4336–4339, 2020. [Online]. Available: https://doi.org/10.1016/j.matpr.2020.07.457

[5] K. K. R. Yadav, A. R. Paul, A. Jain, and F. Alam, "Effects of synthetic jets on swirl inflow in a variable-geometry twin air-intake," *Flow, Turbulence and Combustion*, vol. 111, no. 4, pp. 1193–1225, Sep. 2023. [Online]. Available: https://doi.org/10.1007/s10494-023-00481-8

[6] M. Maddox, *Human Factors Guide for Aviation Maintenance*. Washington, DC: Aviation Medicine, Federal Aviation Administration, U.S. Department of Transportation, 1996. [Online]. Available: https://upsalesiana.ec/ing34ar10r1

[7] M. Tsakalerou, D. Nurmaganbetov, and N. Beltenov, "Aircraft maintenance 4.0 in an era of disruptions," *Procedia Computer Science*, vol. 200, pp. 121–131, 2022. [Online]. Available: https://doi.org/10.1016/j.procs.2022.01.211

[8] D. Xie, M. Xu, and H. Dai, "Effects of damage parametric changes on the aeroelastic behaviors of a damaged panel," *Nonlinear Dynamics*, vol. 97, no. 2, pp. 1035–1050, Jun. 2019. [Online]. Available: https://doi.org/10.1007/s11071-019-05029-y

[9] S. Bowling, S. Kaewkuekool, M. Khasawneh, R. Desai, and K. Gramopadhye, "Confined space work in aircraft maintenance industry: Scope for improving safety and reducing errors," 05 2002. [Online]. Available: https://upsalesiana.ec/ing34ar10r9

[10] M. Verhoeff, W. Verhagen, and R. Curran, "Maximizing operational readiness in military aviation by optimizing flight and maintenance planning," *Transportation Research Procedia*, vol. 10, pp. 941–950, 2015. [Online]. Available: https://doi.org/10.1016/j.trpro.2015.09.048

[11] S. Fu and N. P. Avdelidis, "Prognostic and health management of critical aircraft systems and components: An overview," *Sensors*, vol. 23, no. 19, p. 8124, Sep. 2023. [Online]. Available: https://doi.org/10.3390/s23198124

[12] M. Siegel, P. Gunatilake, and G. Podnar, "Robotic assistants for aircraft inspectors," *Industrial Robot: An International Journal*, vol. 25, no. 6, pp. 389–400, Dec. 1998. [Online]. Available: https://doi.org/10.1108/01439919810240234

[13] Y. Zhang, P. Li, J. Quan, L. Li, G. Zhang, and D. Zhou, "Progress, challenges, and prospects of soft robotics for space applications," *Advanced Intelligent Systems*, vol. 5, no. 3, Jun. 2022. [Online]. Available: https://doi.org/10.1002/aisy.202200071

[14] A. H. Alami, A. Ghani Olabi, A. Alashkar, S. Alasad, H. Aljaghoub, H. Rezk, and M. A. Abdelkareem, "Additive manufacturing in the aerospace and automotive industries: Recent trends and role in achieving sustainable development goals," *Ain Shams Engineering Journal*, vol. 14, no. 11, p. 102516, Nov. 2023. [Online]. Available: https://doi.org/10.1016/j.asej.2023.102516

[15] J. S. Bennett, B. E. Vyhnalek, H. Greenall, E. M. Bridge, F. Gotardo, S. Forstner, G. I. Harris, F. A. Miranda, and W. P. Bowen, "Precision magnetometers for aerospace applications: A review," *Sensors*, vol. 21, no. 16, p. 5568, Aug. 2021. [Online]. Available: https://doi.org/10.3390/s21165568

[16] D. A. Rodríguez, C. Lozano Tafur, P. F. Melo Daza, J. A. Villalba Vidales, and J. C. Daza Rincón, "Inspection of aircrafts and airports using UAS: A review," *Results in Engineering*, vol. 22, p. 102330, Jun. 2024. [Online]. Available: https://doi.org/10.1016/j.rineng.2024.102330

[17] M. Kaur Dhoot, I.-S. Fan, and Z. Skaf, "Review of robotic systems for aircraft inspection," *SSRN Electronic Journal*, 2020. [Online]. Available: https://dx.doi.org/10.2139/ssrn.3718054

[18] J. Shang, T. Sattar, S. Chen, and B. Bridge, "Design of a climbing robot for inspecting aircraft wings and fuselage," *Industrial Robot: An International Journal*, vol. 34, no. 6, pp. 495–502, Oct. 2007. [Online]. Available: http://dx.doi.org/10.1108/01439910710832093

[19] M. Fujita, S. Ikeda, T. Fujimoto, T. Shimizu, S. Ikemoto, and T. Miyamoto, "Development of universal vacuum gripper for wall-climbing robot," *Advanced Robotics*, vol. 32, no. 6, pp. 283–296, Mar. 2018. [Online]. Available: https://doi.org/10.1080/01691864.2018.1447238

[20] Y. L. Silva Vidal, E. D. Supo Colquehuanca, D. F. Meneses Huanca, E. J. Valdeiglesias Flores, F. J. Uchamaco Noa, J. A. Guevara Mamani, J. L. Apaza Gutierrez, and G. W. Galdos Alvarez, "Analysis of robotics applied to mobility in the air intakes of a fighter aircraft," *International Journal of Mechanical Engineering and Robotics Research*, vol. 11, no. 12, pp. 937–947, Dec. 2022, [En línea]. [Online]. Available: https://upsalesiana.ec/ing34ar10r20

[21] D. M. Helevera, *Visual examinations and manual checks to determine the condition of an aircraft and its component.* National Aviation University, Ukraine, 2022. [Online]. Available: https://upsalesiana.ec/ing34ar10r21

[22] S. Kumar Thukaram, *Robot based 3D welding for jet engine blade repair and rapid prototyping of small components.* University of Manitoba, 2010. [Online]. Available: https://upsalesiana.ec/ing34ar10r22

[23] R. M. Groves, *3.12 Inspection and Monitoring of Composite Aircraft Structures.* Elsevier, 2018, pp. 300–311. [Online]. Available: https://doi.org/10.1016/B978-0-12-803581-8.10340-6

[24] M. Bjelonic, V. Klemm, J. Lee, and M. Hutter, *A Survey of Wheeled-Legged Robots.* Springer International Publishing, Aug. 2022, pp. 83–94. [Online]. Available: https://doi.org/10.1007/978-3-031-15226-9_11

[25] T. Klamt, D. Rodríguez, M. Schwarz, C. Lenz, D. Pavlichenko, D. Droeschel, and S. Behnke, "Supervised autonomous locomotion and manipulation for disaster response with a centaur-like robot," in *2018 IEEE/RSJ International Conference on Intelligent Robots and Systems (IROS).* IEEE, Oct. 2018, pp. 1–8. [Online]. Available: https://doi.org/10.1109/IROS.2018.8594509

[26] G. Endo and S. Hirose, "Study on roller-walker – Improvement of locomotive efficiency of quadruped robots by passive wheels," *Advanced Robotics*, vol. 26, no. 8–9, pp. 969–988, May 2012. [Online]. Available: https://doi.org/10.1163/156855312X633066

[27] J. Li, Y. Liu, Z. Yu, Y. Guan, Y. Zhao, Z. Zhuang, and T. Sun, "Design, analysis, and experiment of a wheel-legged mobile robot," *Applied Sciences*, vol. 13, no. 17, p. 9936, Sep. 2023. [Online]. Available: https://doi.org/10.3390/app13179936

[28] J. Niu, H. Wang, Z. Jiang, L. Chen, J. Zhang, Y. Feng, and S. Guo, "Kinematic analysis of a serial-parallel hybrid mechanism and its application to a wheel-legged robot," *IEEE Access*, vol. 8, pp. 111 931–111 944, 2020. [Online]. Available: https://doi.org/10.1109/ACCESS.2020.3001653

[29] F. Raza, W. Zhu, and M. Hayashibe, "Balance stability augmentation for wheel-legged biped robot through arm acceleration control," *IEEE Access*, vol. 9, pp. 54 022–54 031, 2021. [Online]. Available: https://doi.org/10.1109/ACCESS.2021.3071055

[30] Y. Xin, H. Chai, Y. Li, X. Rong, B. Li, and Y. Li, "Speed and acceleration control for a two wheel-leg robot based on distributed dynamic model and whole-body control," *IEEE Access*, vol. 7, pp. 180 630–180 639, 2019. [Online]. Available: https://doi.org/10.1109/ACCESS.2019.2959333

[31] V. S. Medeiros, E. Jelavic, M. Bjelonic, R. Siegwart, M. A. Meggiolaro, and M. Hutter, "Trajectory optimization for wheeled-legged quadrupedal robots driving in challenging terrain," *IEEE Robotics and Automation Letters*, vol. 5, no. 3, pp. 4172–4179, Jul. 2020. [Online]. Available: https://doi.org/10.1109/LRA.2020.2990720

[32] H. Peng, J. Wang, S. Wang, W. Shen, D. Shi, and D. Liu, "Coordinated motion control for a wheel-leg robot with speed consensus strategy," *IEEE/ASME Transactions on Mechatronics*, pp. 1–1, 2020. [Online]. Available: https://doi.org/10.1109/TMECH.2020.2975083